Microenvironment-Responsive Three-Pronged Approach Breaking Traditional Chemotherapy to Target Cancer Stem Cells for Synergistic Inoperable Large Tumor Therapy

Yan Li, Ruilong Zhang, Zhiguo Lu, Guanghui Ma, Lei Chen, Qunwei Tang, and Xin Zhang**

The primary cause for the dismal prognosis of patients with malignant tumors is diagnosis with inoperable disease.[1] For patients with inoperable tumor, traditional chemotherapy is the main method to control tumor growth and inhibit metastasis. However, those patients frequently suffer from terminal stage with large tumor as the traditional chemotherapy is merely focused on differentiated cancer cells.[2] Recently, it has been found that cancer cells reside in several levels of differentiation statuses, including differentiated cancer cells and undifferentiated cancer stem cells (CSCs), especially that large tumors have relatively large number of CSCs.[3] CSCs play an important role in tumor recurrence and metastasis. There is increasing evidence that CSCs are survived with enhanced tumor-reinitiating capacity following standard chemotherapy, which attributes to their intrinsic drug resistant property.[4] Additionally, there is a continual transition between the CSCs and differentiated state.[5] Therefore, anticancer therapies targeting both CSCs and differentiated cancer cells could offer enhanced therapeutic benefits for eradicating large tumor.[6] In light of this, development of strategies to eliminate CSCs and differentiated cancer cells has important clinical significance.

To target CSCs for elimination, it should be noted that they are concentrated in regions with a high density of blood vessels, i.e., "vascular niches."[7] These niches shelter CSCs from apoptosis stimuli and thus allow them to maintain a proper balance.[8] In addition, endothelial cells that line the blood vessels in the vascular niches may secrete factors to promote the survival and self-renewal of CSCs (**Scheme 1**A).[9] Therefore, depletion of vascular niches could reduce the number of CSCs, making them another important target for eradicating large tumor.[10]

In that sense, it is crucial to carry out "three-pronged therapeutic approach" to kill differentiated cancer cells, CSCs, and vascular niches for synergistic inoperable large tumor therapy. In order to kill those three cells simultaneously, drugs irinotecan (Ir), cyclopamine (CP), and erlotinib (ET) targeting differentiated cancer cells, CSCs, and endothelial cells of the vascular niches are used in our system, respectively. Unfortunately, the therapeutic effectiveness of free anticancer drugs is always limited by the ease of blood clearance and poor ability to reach the target cells.[11] Nanoparticles (NPs) that can provide efficient delivery of anticancer drugs to tumor site upon systemic administration are emerging as a promising method to improve cancer treatment.[12] Thus far, however, few three-pronged NPs-based cancer treatments have been reported. Prior studies have focused at most on two of the three. Patel et al. evaluated tariquidar and paclitaxel-loaded long-circulating liposomes targeting differentiated cancer cells, and Zhou's groups used a combination of docetaxel and CP to kill differentiated cancer cells and CSCs.[13] Therefore, it is necessary to develop three-pronged NPs, which can not only deliver anticancer drugs to the tumor site, but also deliver controlled-release drugs to differentiated cancer cells, CSCs, and vascular niches.

To address these challenges, we utilized the intrinsic properties and microenvironment of tumor tissues to develop hypoxia/extracellular pH (pHe)-responsive NPs to achieve three-pronged treatment of inoperable large tumor (Scheme 1B). The tissue partial pressure of oxygen measured from CSCs is near 0 mmHg, which is substantially lower than that of normal tissues (≈30 mmHg).[14] This phenomenon is evident in large tumor with developed areas of hypoxia surrounding CSCs. This unique characteristic indicates that hypoxia might be a primary therapeutic target of azobenzene derivatives, because they are highly sensitive to hypoxia.[15] Following this rationale, a hydrophobic azobenzene

Dr. Y. Li, R. Zhang, Z. Lu, Prof. G. Ma, Prof. X. Zhang
State Key Laboratory of Biochemical Engineering
Institute of Process Engineering
Chinese Academy of Sciences
Beijing 100190, P. R. China
E-mail: xzhang@ipe.ac.cn

R. Zhang, Prof. Q. Tang
Institute of Materials Science and Engineering
Ocean University of China
Qingdao 266100, P. R. China
E-mail: tangqunwei@ouc.edu.cn

Z. Lu
University of Chinese Academy of Science
Beijing 100190, P. R. China

Prof. L. Chen
Department of Obstetrics and Gynecology
Navy General Hospital of People Liberation Army
Beijing 100048, P. R. China

DOI: 10.1002/smll.201601932

© 2016 Wiley-VCH Verlag GmbH & Co. KGaA, Weinheim

www.MaterialsViews.com

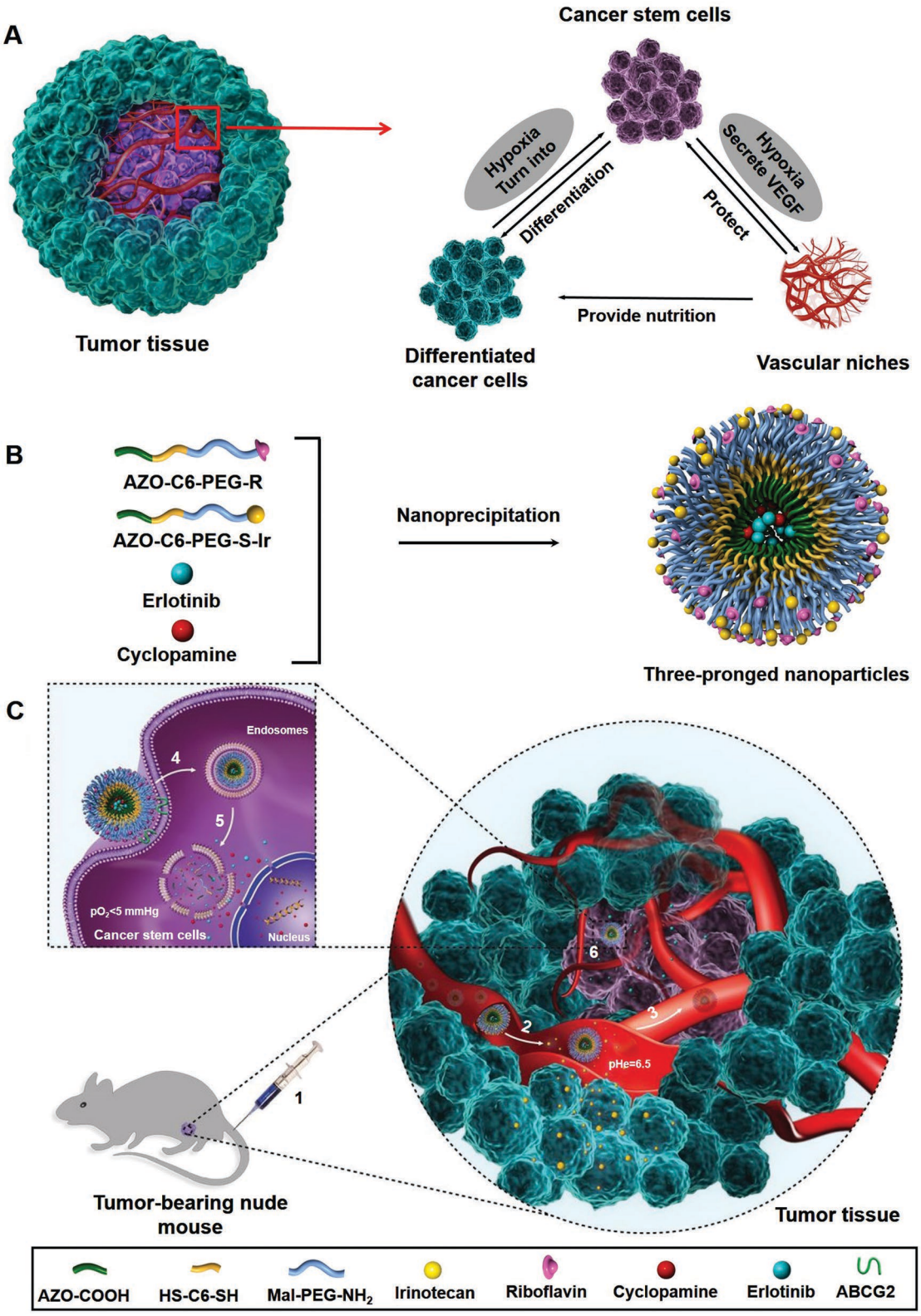

Scheme 1. A) The structure of tumor tissue and the relationship between the differentiated cancer cells, CSCs, and vascular niches. B) The structural composition and preparation of the three-pronged NPs. C) The schematic diagram of cellular uptake and drug release of NPs in tumor. (1) NPs were intravenously injected via the tail vein; (2) NPs accumulated in tumor tissue via the EPR effect and Ir killing differentiated cancer cells on the outlay of NPs was released first due to the acidic labile of amide with β-carboxylic acid group; (3) The system shedding Ir kept integrity to permeate into the inner of tumor tissue; (4) The NPs actively targeted the CSCs via the recognition between R and CSCs; (5) The system could be collapsed immediately due to the hypoxia-responsive of AZO and released drugs of CP to act on CSCs; (6) ET could be released out after the death of CSCs and have function on the vascular niches.

© 2016 Wiley-VCH Verlag GmbH & Co. KGaA, Weinheim

small 2016,
DOI: 10.1002/smll.201601932

derivative 4-(phenylazo) benzoic acid (AZO-COOH) was linked to polyethylene glycol (PEG) to build NPs for loading hydrophobic ET and CP to destroy the vascular niches and kill the CSCs (Figure S1, Supporting Information). As carriers only with target groups, which can specifically recognize and be efficiently internalized by CSCs, could deliver drugs into the cytoplasm of CSCs. It has been demonstrated that riboflavin (R) could be accumulated in CSCs through the membrane-bounded cytoplasmic structures bearing ATP-dependent ABCG2 transporters.[16] To take advantage of this in targeting CSCs, R was linked to the surface of NPs (AZO-C6-PEG-R). Additionally, Ir targeting differentiated cancer cells has to be released before NPs are internalized by CSCs. It is worth noting that the pH of tumor extracellular environment (pHe 6.5) is more acidic than that of the blood and normal tissue (pH 7.4).[17] Therefore, acidic-sensitive amide with β-carboxylic acid group was used to link the hydrophilic Ir to the surface of NPs (AZO-C6-PEG-S-Ir).[18]

So far, hypoxia/pHe-responsive three-pronged NPs targeting CSCs were constructed for delivery of synergistic agents to inoperable large tumor. As shown in Scheme 1C, after systemic administration via the tail vein (1), NPs accumulate in tumor tissue via the enhanced permeability and retention (EPR) effect. Ir killing differentiated cancer cells is released from the NPs surface because of acidic labile of amide with β-carboxylic acid group (2). The integrity of the release system is maintained after releasing Ir (3), and NPs permeate the tumor tissue to actively target CSCs via the recognition between R and CSCs. After endocytosis into CSCs (4), the carrier system collapses immediately due to the hypoxia-responsive of AZO with release of CP and ET (5). After the death of CSCs induced by CP, ET is released to target vascular niches (6). With spatially and temporally controlled ability, three-pronged NPs targeting CSCs are expected to prevent their longevity and synergistically inhibit inoperable large tumors.

The chemical composition of purified intermediates and end products was studied by ^{1}H NMR spectra (Figure S2, Supporting Information), which confirmed the successful synthesis of the hypoxia/pHe-responsive AZO-C6-PEG-S-Ir and CSCs-targeting AZO-C6-PEG-R molecules. Products that are not hypoxia-responsive, namely, biphenyl-4-carboxylic acid (BCA)-based BCA-C6-PEG-S-Ir and BCA-C6-PEG-R, and those are not pHe-responsive ester bond linked AZO-C6-PEG-N-Ir, were also successfully synthesized as controls.

Next, hypoxia/pHe-responsive NPs with CSCs-targeting R encapsulating CP and ET [$^{(ET+CP)}NP_{(AZO\text{-}S\text{-}Ir/R)}$] were constructed for inoperable large tumor therapy. As displayed in Table S1 (Supporting Information), non-pHe-responsive $^{(ET+CP)}NP_{(AZO\text{-}N\text{-}Ir/R)}$, non-hypoxia-responsive $^{(ET+CP)}NP_{(BCA\text{-}S\text{-}Ir/R)}$, non-targeting $^{(ET+CP)}NP_{(AZO\text{-}S\text{-}Ir)}$, and NPs encapsulating only one drug or without a drug [$^{(CP)}NP_{(AZO\text{-}S\text{-}Ir/R)}$, $^{(ET)}NP_{(AZO\text{-}S\text{-}Ir/R)}$, and $NP_{(AZO\text{-}S\text{-}Ir/R)}$] were prepared as controls. Comprehensive characterizations were conducted to evaluate the physicochemical properties of all NPs. Dynamic light scattering (DLS) measurement showed that the average diameter of all NPs was about 40 nm (**Figure 1**A), with a polydispersity index of ≈0.2 (Figure S3, Supporting Information), indicating the superior tumor accumulation ability via the EPR effect.[19] The low zeta potential

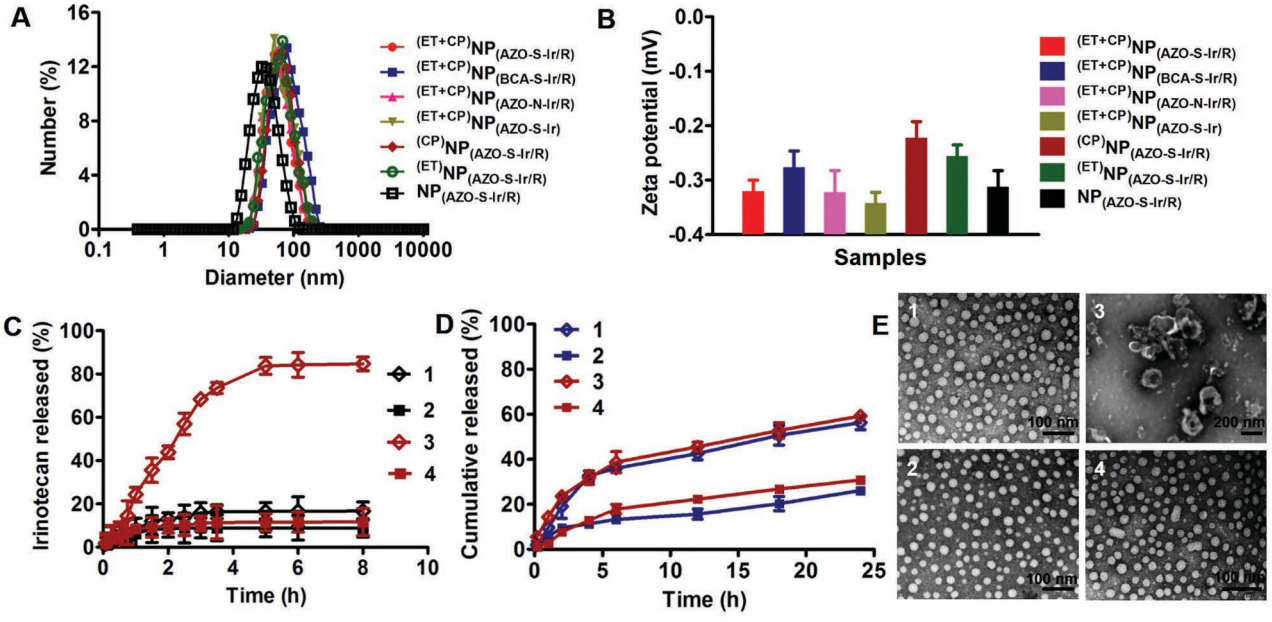

Figure 1. The characterization of NPs. A) The size distribution of NPs. B) The zeta potential of NPs. C) The Ir released of different NPs at different conditions at 37 °C. (1) $^{(ET+CP)}NP_{(AZO\text{-}S\text{-}Ir/R)}$ pH = 7.4; (2) $^{(ET+CP)}NP_{(AZO\text{-}N\text{-}Ir/R)}$ pH = 7.4; (3) $^{(ET+CP)}NP_{(AZO\text{-}S\text{-}Ir/R)}$ pH = 6.5; (4) $^{(ET+CP)}NP_{(AZO\text{-}N\text{-}Ir/R)}$ pH = 6.5. D) The cumulative released of ET and CP for different NPs with rat liver microsome enzymes and NADPH at 37 °C. (1) ET of $^{(ET+CP)}NP_{(AZO\text{-}S\text{-}Ir/R)}$; (2) ET of $^{(ET+CP)}NP_{(BCA\text{-}S\text{-}Ir/R)}$; (3) CP of $^{(ET+CP)}NP_{(AZO\text{-}S\text{-}Ir/R)}$; (4) CP of $^{(ET+CP)}NP_{(BCA\text{-}S\text{-}Ir/R)}$. E) The morphology of NPs before and after treating with rat liver microsome enzymes and NADPH at 37 °C. (1) $^{(ET+CP)}NP_{(AZO\text{-}S\text{-}Ir/R)}$ before treatment; (2) $^{(ET+CP)}NP_{(BCA\text{-}S\text{-}Ir/R)}$ before treatment; (3) $^{(ET+CP)}NP_{(AZO\text{-}S\text{-}Ir/R)}$ after treatment; (4) $^{(ET+CP)}NP_{(BCA\text{-}S\text{-}Ir/R)}$ after treatment. The mean ± SD is shown (n = 3).

DOI: 10.1002/smll.201601932
© 2016 Wiley-VCH Verlag GmbH & Co. KGaA, Weinheim

(Figure 1B) ensured the stability of all NPs in an environment containing 10% fetal bovine serum (FBS) due to the modification of PEG (Figure S4, Supporting Information).

The release experiments of Ir were performed at pH 7.4 and 6.5 simulating the physiological and tumor extracellular environments, respectively. From the graph in Figure 1C, the release of Ir from $^{(ET+CP)}NP_{(AZO\text{-}S\text{-}Ir/R)}$ (1) and $^{(ET+CP)}NP_{(AZO\text{-}N\text{-}Ir/R)}$ (2) was negligible at pH 7.4 for 8 h, indicating stability in the physiological environment. The amount of Ir released from $^{(ET+CP)}NP_{(AZO\text{-}S\text{-}Ir/R)}$ (3) reached 84.7% after 8 h incubation at pH 6.5, whereas it was only 11.6% for the ester bond linked $^{(ET+CP)}NP_{(AZO\text{-}N\text{-}Ir/R)}$ (4). Results indicated that Ir could be quickly released in the tumor extracellular environment on account of the weakly acid-responsive amide with β-carboxylic acid group of $^{(ET+CP)}NP_{(AZO\text{-}S\text{-}Ir/R)}$. Furthermore, transmission electron microscope (TEM) images (Figure S5, Supporting Information) confirmed that most of the $^{(ET+CP)}NP_{(AZO\text{-}S\text{-}Ir/R)}$ retained their integrity after releasing Ir, which would allow permeation within the tumor tissue.

To evaluate the effect of hypoxia on NPs, the release profiles of encapsulated ET and CP were detected after treating NPs with rat liver microsome enzymes and reduced nicotinamide adenine dinucleotide phosphate (NADPH). It was clear that 56.2% of ET was released from $^{(ET+CP)}NP_{(AZO\text{-}S\text{-}Ir/R)}$ after 24 h incubation, while only 25.8% from $^{(ET+CP)}NP_{(BCA\text{-}S\text{-}Ir/R)}$ (Figure 1D). Additionally, the release profiles of CP showed the same trend. The morphology of NPs after treatment for 2 min was also taken via TEM. Figure 1E showed that both $^{(ET+CP)}NP_{(AZO\text{-}S\text{-}Ir/R)}$ (1) and $^{(ET+CP)}NP_{(BCA\text{-}S\text{-}Ir/R)}$ (2) were monodispersed and spherical-like structures before treatment. The AZO bond linked $^{(ET+CP)}NP_{(AZO\text{-}S\text{-}Ir/R)}$ immediately collapsed within 2 min of treatment (3), whereas the BCA linked $^{(ET+CP)}NP_{(BCA\text{-}S\text{-}Ir/R)}$ kept integrity (4). The disappearance of red shift for the π–π^* band of the AZO bond after enzyme treatment (Figure S6, Supporting Information) further confirmed the breakage of AZO bonds in a hypoxic environment, resulting in the disassembly of NPs and the prompt release of encapsulated drugs.

To further evaluate the effect of NPs on differentiated cancer cells, endothelial cells of vascular niches, and CSCs, MCF-7 cancer cells were used as model. Differentiated cancer cells, human umbilical vein endothelial cells (HUVECs), and MCF-7 mammospheres were co-cultured in transwell chambers to mimic the tumor tissue (**Figure 2**A) and Cy5 was used as a fluorescence probe instead of CP and ET. The distribution of drugs in targeted cells was observed by confocal laser scanning microscope (CLSM). As shown in Figure 2B and Figure S7A (Supporting Information), pretreatment in a weakly acidic environment (pHe = 6.5) for 4 h resulted in extensive distribution of Ir autofluorescence in MCF-7 differentiated cancer cells with pHe-sensitive $^{(Cy5)}NP_{(AZO\text{-}S\text{-}Ir/R)}$ and $^{(Cy5)}NP_{(AZO\text{-}S\text{-}Ir)}$. In comparison, almost no Ir was detected in MCF-7 differentiated cancer cells for $^{(Cy5)}NP_{(AZO\text{-}N\text{-}Ir/R)}$ as PEG modification reduced the interaction of NPs with differentiated cancer cells and NPs could not release free Ir at pHe 6.5. As expected, the mean fluorescence intensity of Cy5 in CSCs with $^{(Cy5)}NP_{(AZO\text{-}S\text{-}Ir/R)}$ and $^{(Cy5)}NP_{(AZO\text{-}N\text{-}Ir/R)}$ modified with R was 2.2 and 3.0 times the free Cy5 and $^{(Cy5)}NP_{(AZO\text{-}S\text{-}Ir)}$ without R, respectively (Figure S7B, Supporting Information). These data indicated that only the pHe-sensitive $^{(Cy5)}NP_{(AZO\text{-}S\text{-}Ir/R)}$ could achieve specific distribution of Ir in differentiated cancer cells, and that R could facilitate cellular uptake of NPs by CSCs via the recognition between R and ABCG2 transporters.

To further confirm that R modification enhanced the permeability of NPs, the distribution of Cy5 in MCF-7 CSCs mammospheres was observed in 3D. As shown in Figure 2C,D, the mean fluorescence intensity of Cy5 at each distance for R modified $^{(Cy5)}NP_{(AZO\text{-}S\text{-}Ir/R)}$ was much higher than that for free Cy5 and $^{(Cy5)}NP_{(AZO\text{-}S\text{-}Ir)}$ without R. It was 23.4 for $^{(Cy5)}NP_{(AZO\text{-}S\text{-}Ir/R)}$ at a depth of 15 μm, but only 10.8 and 8.2 for $^{(Cy5)}NP_{(AZO\text{-}S\text{-}Ir)}$ and free Cy5, respectively. The results indicated that R modification not only achieved active targeting of $^{(Cy5)}NP_{(AZO\text{-}S\text{-}Ir/R)}$ to CSCs, but could also facilitate the permeability of NPs to the inner of CSCs mammospheres.

The tumorigenic potential of CSCs is associated with self-renewal capacity to initiate tumor growth and spread. Mammospheres forming assay was used to characterize the effect of NPs treatment on CSCs. As shown in Figure 2E, phosphate buffered saline (PBS), empty $NP_{(AZO\text{-}S\text{-}Ir/R)}$, and non-hypoxia $^{(ET+CP)}NP_{(BCA\text{-}S\text{-}Ir/R)}$ conserved the ability of MFC-7 CSCs to form mammospheres, whereas the hypoxia-responsive $^{(ET+CP)}NP_{(AZO\text{-}S\text{-}Ir/R)}$, $^{(ET+CP)}NP_{(AZO\text{-}S\text{-}Ir)}$, and free drugs caused drastic reductions in the size of mammospheres. Treatment with $^{(ET+CP)}NP_{(AZO\text{-}S\text{-}Ir/R)}$ resulted in the strongest inhibition (77.0%) thanks to their increased cellular uptake and permeability.

The inhibitory effect of the three-pronged NPs on cell proliferation was evaluated in transwell chambers using 3-(4,5-dimethylthiazol-2-yl)-2,5-diphenyl tetrazolium bromide (MTT) assay. As shown in Figure 2F, compared with PBS control (1), the survival rate of MCF-7 differentiated cancer cells was reduced to around 20% by $^{(ET+CP)}NP_{(AZO\text{-}S\text{-}Ir/R)}$ (2), other pHe-sensitive NPs (3, 4, 5, 7, 8) and free Ir (9, 12), whereas it was about 90% for the non-pHe-sensitive $^{(ET+CP)}NP_{(AZO\text{-}N\text{-}Ir/R)}$ (6), free ET (10), and CP (11). The results indicated that Ir linked with amide with β-carboxylic acid group could be released in an acidic environment and had an inhibitory effect on differentiated cancer cells as free Ir. The cell viability of MCF-7 CSC mammospheres was different that only $^{(ET+CP)}NP_{(AZO\text{-}S\text{-}Ir/R)}$ (2), $^{(CP)}NP_{(AZO\text{-}N\text{-}Ir/R)}$ (5), and $^{(ET+CP)}NP_{(AZO\text{-}N\text{-}Ir/R)}$ (6) with AZO and R loading CP had inhibitory effect of ≈80.0%. The effect was much greater than that observed with other NPs (Figure 2G). The cell viability of HUVECs treated with $^{(ET)}NP_{(AZO\text{-}S\text{-}Ir/R)}$ was ≈51.2%, which was higher than that observed with $^{(ET+CP)}NP_{(AZO\text{-}S\text{-}Ir/R)}$ (2) and $^{(ET+CP)}NP_{(AZO\text{-}N\text{-}Ir/R)}$ (6) containing ET and CP (Figure 2H). The reason was that only $^{(ET+CP)}NP_{(AZO\text{-}S\text{-}Ir/R)}$ (2) and $^{(ET+CP)}NP_{(AZO\text{-}N\text{-}Ir/R)}$ (6) inducing the apoptosis of CSCs could release ET efficiently to kill HUVECs. Taken together these three results, only $^{(ET+CP)}NP_{(AZO\text{-}S\text{-}Ir/R)}$ (2) with pHe/hypoxia-responsive loading with three drugs could simultaneously inhibit the proliferation of differentiated cancer cells, CSCs, and HUVECs.

We next investigated whether the enhanced delivery of drug CP into CSCs could reduce the stemness in breast

© 2016 Wiley-VCH Verlag GmbH & Co. KGaA, Weinheim

DOI: 10.1002/smll.201601932

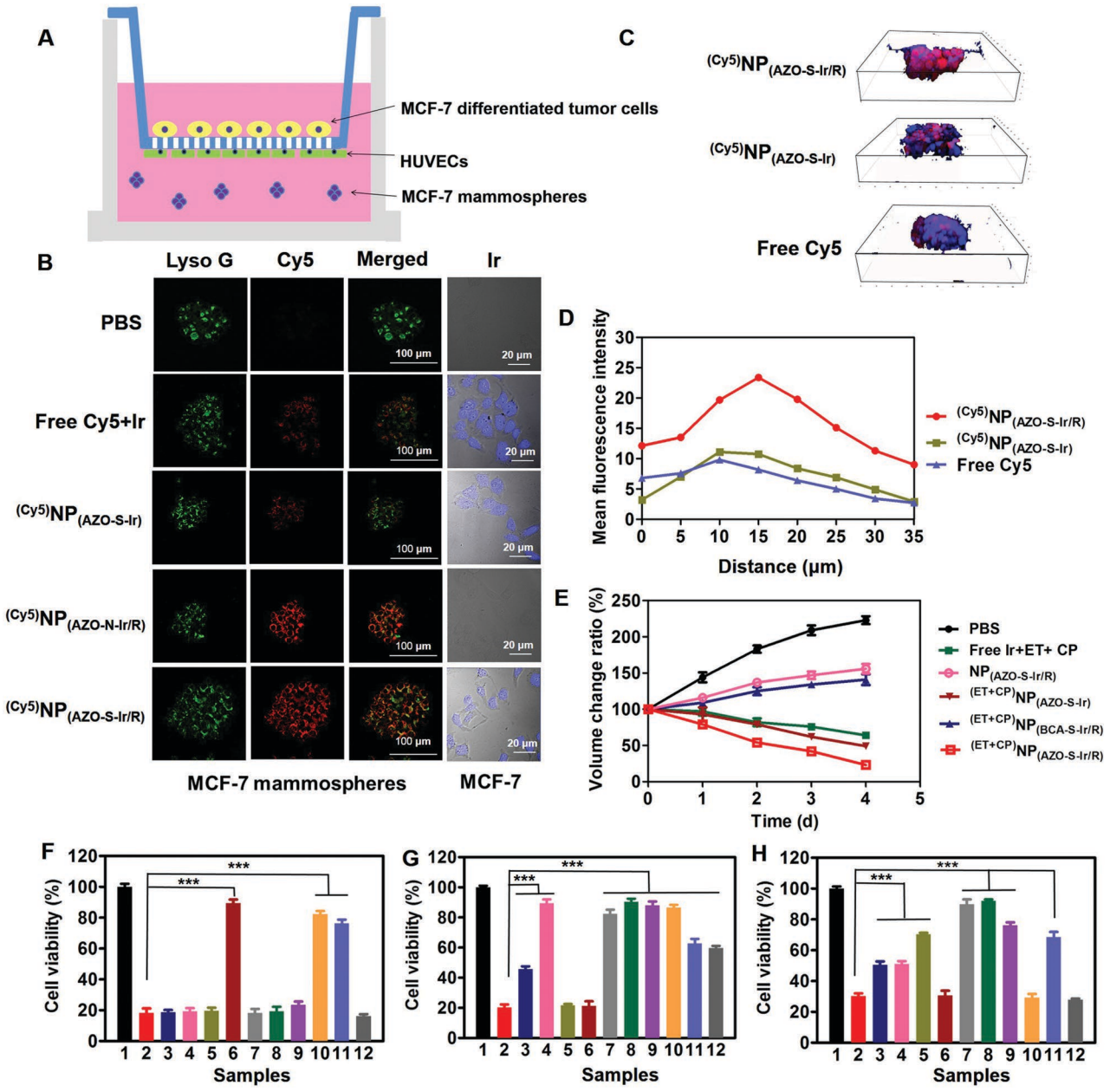

Figure 2. A) The structure of transwell chamber. MCF-7 differentiated cancer cells, HUVECs, and MCF-7 mammospheres were co-cultured in transwell chamber imitating tumor tissue. B) The distribution of drugs in MCF-7 differentiated cancer cells and CSCs mammospheres were observed by confocal laser scanning microscopy (CLSM). Endosomes/lysosomes were stained with Lysotracker Green. C) The distribution of Cy5 in MCF-7 CSCs mammospheres was observed in 3D. Nuclei were stained with DAPI. D) The mean fluorescence intensity of Cy5 with the extension of distance quantified with software of CLSM. E) The mammospheres forming assay to detect the volume change ratio of CSCs mammospheres after treating with different formulations of drugs. F) The cell viability of MCF-7 differentiated cancer cells after 48 h treatment with different NPs and free drugs. G) The cell viability of MCF-7 CSCs mammospheres after 48 h treatment with different NPs and free drugs. H) The cell viability of HUVECs after 48 h treatment with different NPs and free drugs. Samples: (1) PBS; (2) $^{(ET+CP)}NP_{(AZO\text{-}S\text{-}Ir/R)}$; (3) $^{(ET+CP)}NP_{(AZO\text{-}S\text{-}Ir)}$; (4) $^{(ET)}NP_{(AZO\text{-}S\text{-}Ir/R)}$; (5) $^{(CP)}NP_{(AZO\text{-}S\text{-}Ir/R)}$; (6) $^{(ET+CP)}NP_{(AZO\text{-}N\text{-}Ir/R)}$; (7) $^{(ET+CP)}NP_{(BCA\text{-}S\text{-}Ir/R)}$; (8) $NP_{(AZO\text{-}S\text{-}Ir/R)}$; (9) free Ir; (10) free ET; (11) free CP; (12) free Ir+ET+CP. The mean ± SD is shown ($n = 3$). ***$P < 0.005$.

mammosphere cells in vivo. MCF-7 mammospheres pretreated with NPs or free CP in vitro were implanted into nude mice for tumor formation. As shown in **Figure 3**A, no tumor growth was observed when mice received MCF-7 mammosphere pretreated with $^{(ET+CP)}NP_{(AZO\text{-}S\text{-}Ir/R)}$ and $^{(CP)}NP_{(AZO\text{-}S\text{-}Ir/R)}$. On the contrary, no significant delay in tumor formation was observed in other groups. These results suggested that $NP_{(AZO\text{-}S\text{-}Ir/R)}$ with CP treatment can directly affect MCF-7 CSCs in vivo, resulting in prolonged tumor suppression.

In order to evaluate the potential antitumor activity, we investigated the pharmacokinetics and biodistribution of NPs in vivo. As shown in Figure S8 (Supporting Information), the concentration of encapsulated ET for $^{(ET+CP)}NP_{(AZO\text{-}S\text{-}Ir)}$ was much higher than free drug at designed time point. It was 20 687.42 ng mL^{-1} for $^{(ET+CP)}NP_{(AZO\text{-}S\text{-}Ir)}$ after 5 min injection,

© 2016 Wiley-VCH Verlag GmbH & Co. KGaA, Weinheim

www.MaterialsViews.com

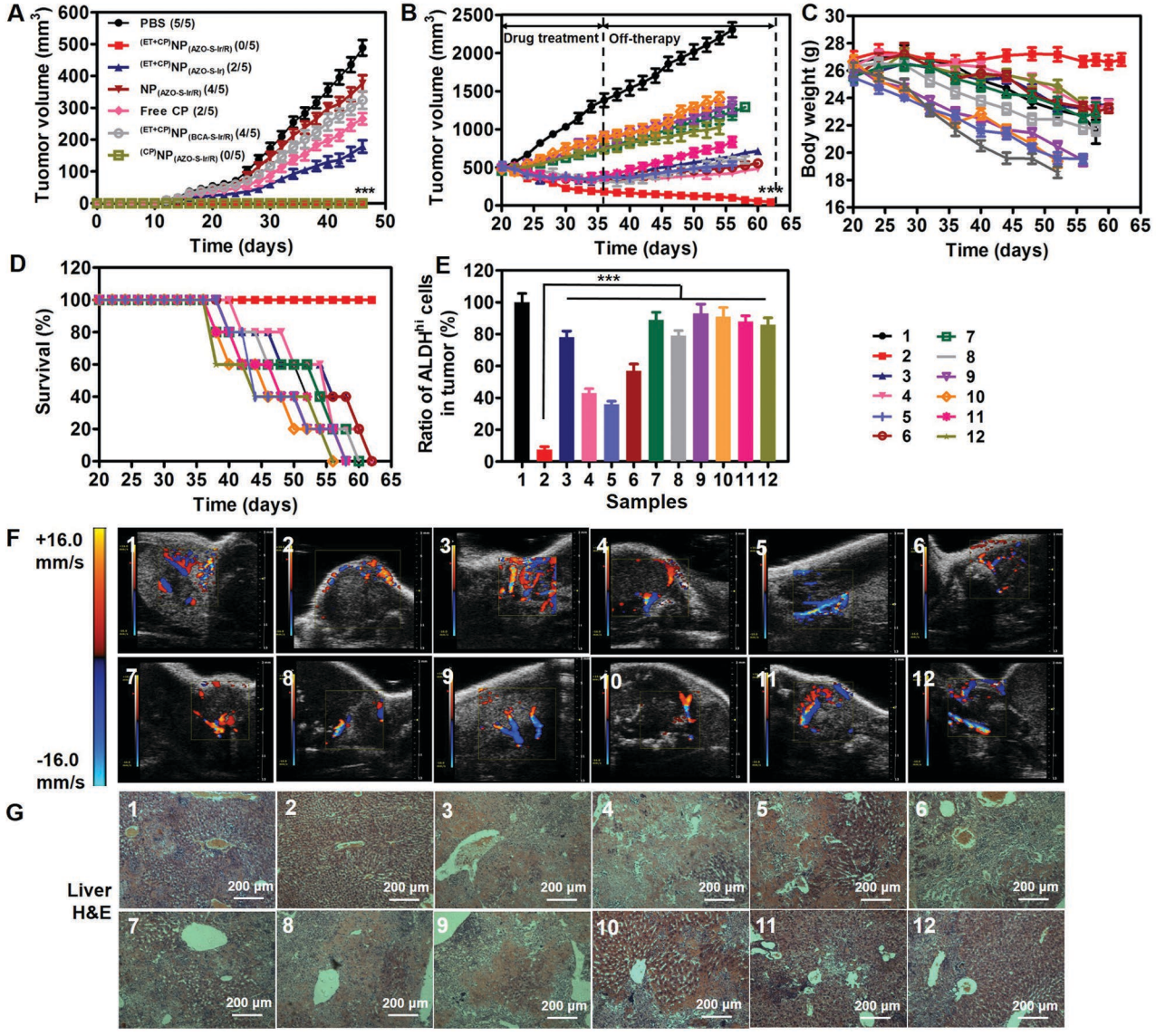

Figure 3. A) Inhibition on tumor formation of MCF-7 cancer stem cells in nude mice pretreated with different formulations in vitro. B) Inhibition on MCF-7 xenograft tumor growth after treatment with different formulations via the tail vein. C) Body weight of MCF-7 tumor-bearing nude mice after treatment. D) Survival curves of MCF-7 tumor-bearing nude mice after treatment. E) The CSCs ratio within MCF-7 tumor after the tumor suppression study. F) 2D color Doppler images of tumor after the tumor suppression study. G) H&E staining of liver sections collected from different groups of mice after the tumor suppression study. Samples: (1) PBS; (2) $^{(ET+CP)}NP_{(AZO\text{-}S\text{-}Ir/R)}$; (3) $^{(ET+CP)}NP_{(AZO\text{-}S\text{-}Ir)}$; (4) $^{(ET)}NP_{(AZO\text{-}S\text{-}Ir/R)}$; (5) $^{(CP)}NP_{(AZO\text{-}S\text{-}Ir/R)}$; (6) $^{(ET+CP)}NP_{(AZO\text{-}N\text{-}Ir/R)}$; (7) $^{(ET+CP)}NP_{(BCA\text{-}S\text{-}Ir/R)}$; (8) $NP_{(AZO\text{-}S\text{-}Ir/R)}$; (9) free Ir; (10) free ET; (11) free CP; (12) free Ir+ET+CP. ***$P < 0.005$.

while only 7430.05 ng mL^{-1} for free drug. The results indicated that $^{(ET+CP)}NP_{(AZO\text{-}S\text{-}Ir)}$ could significantly extend the circulation time of free drug. Furthermore, $^{(Cy5)}NP_{(AZO\text{-}S\text{-}Ir/R)}$ with R enhanced the tumor accumulation compared with free Cy5 and $^{(Cy5)}NP_{(AZO\text{-}S\text{-}Ir)}$ due to their active recognition of CSCs (Figure S9A, Supporting Information). The mean fluorescence intensity of Cy5 for $^{(Cy5)}NP_{(AZO\text{-}S\text{-}Ir/R)}$ in tumor tissue was 1.5 and 1.3 times that for free Cy5 and $^{(Cy5)}NP_{(AZO\text{-}S\text{-}Ir)}$, respectively (Figure S9B, Supporting Information), which indicated the potential benefit for tumor therapy.

To further evaluate the in vivo antitumor effectiveness of $^{(ET+CP)}NP_{(AZO\text{-}S\text{-}Ir/R)}$, MCF-7 tumor-bearing nude mice were treated with different formulations via intravenous injection of equivalent drug doses of 0.25 mg ET kg^{-1}, 0.25 mg CP kg^{-1}, and 0.8 mg Ir kg^{-1}. Tumors grown to ≈500 mm^3 were used as an inoperable large tumor model. Treatment was divided into two stages including the administration of seven daily doses every other day followed by an off-therapy stage. As shown in Figure 3B, treatments with other formulations at the same effective doses only moderately inhibited tumor growth, and there was an obvious recurrence during the off-therapy stage. In contrast, treatment with pHe/hypoxia-responsive three-pronged $^{(ET+CP)}NP_{(AZO\text{-}S\text{-}Ir/R)}$ (2) significantly reduced tumor growth from 497.8 to 45.3 mm^3 with no recurrence during the off-therapy stage. The in vivo results demonstrated effective inhibition of tumor growth by the pHe/hypoxia-responsive three-pronged $^{(ET+CP)}NP_{(AZO\text{-}S\text{-}Ir/R)}$.

© 2016 Wiley-VCH Verlag GmbH & Co. KGaA, Weinheim
small 2016,
DOI: 10.1002/smll.201601932

Mice treated with NPs other than $^{(ET+CP)}NP_{(AZO\text{-}S\text{-}Ir/R)}$ groups experienced severe weight loss, which was due to the differences in therapeutic effectiveness (Figure 3C). Moreover, the survival rate of mice treated with $^{(ET+CP)}NP_{(AZO\text{-}S\text{-}Ir/R)}$ was the highest among all groups (Figure 3D).

Subsequently, we analyzed the effect of NPs on CSCs, vascular niches, and differentiated cancer cells. The percentage of CSCs was marked with $ALDH^{hi}$ in the MCF-7 tumor models at the end of drug treatment stage. As shown in Figure 3E, $^{(ET+CP)}NP_{(AZO\text{-}S\text{-}Ir/R)}$ treatment resulted in a decrease in the percentage of CSCs in the population of residual tumor cells to 10.2% of that in response to PBS treatment (set as 100%). Figure 3F showed the color Doppler images of tumor after treatment. Blood flow is clearly shown in tumor treated with PBS and NPs other than $^{(ET+CP)}NP_{(AZO\text{-}S\text{-}Ir/R)}$. Nearly no blood flow is apparent in the centers of tumor following treating with $^{(ET+CP)}NP_{(AZO\text{-}S\text{-}Ir/R)}$ owing to their increased permeability and the destruction of blood vessels. Notably, $^{(ET+CP)}NP_{(AZO\text{-}S\text{-}Ir/R)}$ treatment was associated with the highest level of tumor cell apoptosis as shown by terminal deoxynucleotidyltransferase mediated UTP end labeling (TUNEL) analyses and hematoxylin and eosin (H&E) staining (Figure S10, Supporting Information). In addition, the H&E staining (Figure 3G) of the liver tissues indicated that only mice treated with $^{(ET+CP)}NP_{(AZO\text{-}S\text{-}Ir/R)}$ had almost no cell necrosis and inflammation. These data demonstrated that the pHe/hypoxia-responsive three-pronged $^{(ET+CP)}NP_{(AZO\text{-}S\text{-}Ir/R)}$ significantly inhibited tumors by inducing apoptosis and synergistically prohibit the proliferation of differentiated cancer cells, CSCs, and endothelial cells.

In summary, we successfully developed hypoxia/pHe-responsive three-pronged NPs that could significantly inhibit cell proliferation in large tumor. The $^{(ET+CP)}NP_{(AZO\text{-}S\text{-}Ir/R)}$ could achieve spatially and temporally controlled release of drugs at targeted sites. Ir was released in tumor extracellular environment on account of the weakly acid-responsiveness of amide with β-carboxylic acid group. The hypoxia-responsiveness of AZO led to disassembly of NPs and rapid release of encapsulated drugs within CSCs. In addition, target molecule R achieved active targeting of NPs to CSCs, and facilitated the permeability of NPs to the inner of CSCs mammospheres. Therefore, the three-pronged NPs with pHe/hypoxia-responsive targeting CSCs induced the apoptosis of differentiated cancer cells and CSCs, particularly the $^{(ET+CP)}NP_{(AZO\text{-}S\text{-}Ir/R)}$ could simultaneously destroy the vascular niches in MCF-7 tumor-bearing nude mice. Most importantly, the three-pronged $^{(ET+CP)}NP_{(AZO\text{-}S\text{-}Ir/R)}$ inhibited the growth of large tumor without recurrence. Therefore, three-pronged $^{(ET+CP)}NP_{(AZO\text{-}S\text{-}Ir/R)}$ might have the potential to open up a new avenue for inoperable large tumor treatment.

Supporting Information

Supporting Information is available from the Wiley Online Library or from the author.

Acknowledgements

Y.L. and R.Z. contributed equally to this work. This work was financially supported by the Beijing Natural Science Foundation (2164071), the National Natural Science Foundation of China (31522023, 51373177), the National High Technology Research and Development Program (2014AA020708), the Instrument Developing Project of the Chinese Academy of Sciences (YZ201313), and the Strategic Priority Research Program of the Chinese Academy of Sciences (XDA09030301-3). All procedures involving experimental animals were performed in accordance with protocols approved by the Institutional Animals Care and Use Committee of Peking University.

[1] J. H. Muchmore, J. E. Preslan, W. J. George, *Cancer* **1996**, *78*, 664.

[2] a) B. J. Morrison, C. W. Schmidt, S. R. Lakhi, B. A. Reynolds, J. A. Lopez, *Breast Cancer Res.* **2008**, *10*, 1; b) H. Cleves, *Nat. Med.* **2011**, *17*, 313; c) T. Reya, S. J. Morrision, M. F. Clarke, I. L. Weissman, *Nature* **2001**, *414*, 105; d) E. Charafe-Jauffret, C. Ginestier, F. Iovino, J. Wicinski, N. Cervera, P. Finetti, M. H. Hur, M. E. Diebel, F. Monville, J. Dutcher, M. Brown, P. Viens, L. Xerri, F. Bertucci, G. Stassi, G. Dontu, D. Birnbaum, M. S. Wicha, *Cancer Res.* **2009**, *69*, 1302; e) F. Li, B. Tiede, J. Massague, Y. Kang, *Cell Res.* **2007**, *17*, 3.

[3] H. Korkaya, S. L. Liu, M. S. Wicha, *J. Clin. Invest.* **2011**, *121*, 3804.

[4] S. Chuthapisith, J. Eremin, M. EI-Sheemey, O. Eremin, *Surg. Oncol.* **2010**, *19*, 27.

[5] a) C. L. Chaffer, I. Brueckmann, C. Scheel, A. J. Kaestli, P. A. Wiggins, L. O. Rodrigues, M. Brooksa, F. Reinhardta, Y. Suc, K. Polyakc, L. M. Arendtd, C. Kuperwasserd, B. Bieriea, R. A. Weinberg, *Proc. Natl. Acad. Sci. USA* **2011**, *108*, 7950; b) P. B. Gupa, C. M. Fillmore, G. Z. Jiang, S. D. Shapria, K. Tao, C. Kuperwasser, E. S. Lander, *Cell* **2011**, *146*, 633.

[6] D. Klevebring, G. Rosin, R. Ma, J. Lindberg, K. Czene, J. Kere, I. Fredriksson, J. Bergh, J. Hartman, *Breast Cancer Res.* **2014**, *16*, R72.

[7] a) C. Calabrese, H. Poppleton, M. Kocak, T. L. Hogg, C. Fuller, B. Hamner, E. Y. Oh, M. W. Gaber, D. Finklestein, M. Allen, A. Frank, I. T. Bayazitov, S. S. Zakharenko, A. Gajjar, A. Davidoff, R. J. Gilbertson, *Cancer Cell* **2007**, *11*, 69; b) T. Reya, S. J. Morrison, M. F. Clarke, I. L. Weissman, *Nature* **2001**, *414*, 105.

[8] Z. J. Yang, R. J. Wechsler-Reya, *Cancer Cell* **2007**, *11*, 3.

[9] R. K. Ambasta, A. Sharma, P. Kumar, *Vasc. Cell* **2011**, *3*, 1.

[10] S. J. Conley, E. Gheordunescu, P. Kakarala, B. Newman, H. Korkaya, A. N. Heath, S. G. Clouthier, M. S. Wicha, *Proc. Natl. Acad. Sci. USA* **2012**, *109*, 2784.

[11] Y. Q. Shen, E. L. Jin, B. Zhang, C. J. Murphy, M. H. Sui, J. Zhao, J. Q. Wang, J. B. Tang, M. H. Fan, E. V. Kirk, W. J. Murdoch, *J. Am. Chem. Soc.* **2010**, *132*, 4259.

[12] a) M. N. Holme, I. A. Fedotenko, D. Abegg, J. Althaus, L. Babel, F. Favarger, R. Reiter, R. Tanasescu, P. L. Zaffalon, A. Ziegler, B. Müller, T. Saxer, A. Zumbuehl, *Nat. Nanotechnol.* **2012**, *7*, 536; b) J. Song, J. Zhou, H. Duan, *J. Am. Chem. Soc.* **2012**, *134*, 13458; c) Y. Wang, T. Yang, H. T. Ke, A. J. Zhu, Y. Y. Wang, J. X. Wang, J. K. Shen, G. Liu, C. Y. Chen, Y. L. Zhao, H. B. Chen, *Adv. Mater.* **2015**, *27*, 3874.

[13] a) N. R. Patel, A. Rathi, D. Mongayt, V. P. Torchilin, *Int. J. Pharm.* **2011**, *416*, 296; b) Y. Zhou, J. Y. Yang, J. S. Rhim, J. Kopeček, *J. Controlled Release* **2013**, *172*, 946.

© 2016 Wiley-VCH Verlag GmbH & Co. KGaA, Weinheim

[14] a) W. R. Wilson, M. P. Hay, *Nat. Rev. Cancer* **2011**, *11*, 393; b) A. L. Harris, *Nat. Rev. Cancer* **2002**, *2*, 38; c) J. M. Brown, W. R. Wilson, *Nat. Rev. Cancer* **2004**, *4*, 437.
[15] a) Y. Liu, Y. Xu, X. Qian, J. Liu, L. Shen, J. Li, Y. Zhang, *Bioorg. Med. Chem.* **2006**, *14*, 2935; b) L. Cui, Y. Zhong, W. Zhu, Y. Xu, Q. Du, X. Wang, X. Qian, Y. Xiao, *Org. Lett.* **2011**, *13*, 928; c) K. Xu, F. Wang, X. Pan, R. Liu, J. Ma, F. Kong, B. Tang, *Chem. Commun.* **2013**, *49*, 2554.
[16] I. Miranda-Lorenzo, J. Dorado, E. Lonardo, S. Alcala, A. G. Serrano, J. Clausell-Tormos, M. Cioffi, D. Megias, S. Zagorac, A. Balic, M. Hidalgo, M. Erkann, J. Kleeff, A. Scarpa, B. Sainz Jr., C. Heeschen, *Nat. Methods* **2014**, *11*, 1161.
[17] a) J. Z. Du, X. J. Du, C. Q. Mao, J. Wang, *J. Am. Chem. Soc.* **2011**, *133*, 17560; b) X. Guo, X. Wei, Y. T. Jing, S. B. Zhou, *Adv. Mater.* **2015**, *27*, 6450.
[18] Z. X. Zhou, Y. Q. Shen, J. B. Tang, M. H. Fan, E. A. V. Kirk, W. J. Murdoch, M. Radosz, *Adv. Funct. Mater.* **2009**, *19*, 3580.
[19] Y. Li, R. Y. Liu, J. Yang, Y. J. Shi, G. H. Ma, Z. Z. Zhang, X. Zhang, *Biomaterials* **2015**, *41*, 1.

Received: June 8, 2016
Revised: July 20, 2016
Published online:

© 2016 Wiley-VCH Verlag GmbH & Co. KGaA, Weinheim

DOI: 10.1002/smll.201601932